Research in Veterinary Science 156 (2023) 66–80

Contents lists available at ScienceDirect

Research in Veterinary Science

journal homepage: www.elsevier.com/locate/rvsc

Load-bearing composite fracture-fixation devices with tailored fibre placement for toy-breed dogs

Niko Moritz [a,b], Oliver Liesmäki [a,b], Artem Plyusnin [a,b], Pauli Keränen [c], Julia Kulkova [a,b,*]

[a] Biomedical Engineering Research Group, Biomaterials and Medical Device Research Program, Itäinen Pitkäkatu 4B (PharmaCity), 20520 Turku, Finland
[b] Department of Biomaterials Science and Turku Clinical Biomaterials Centre – TCBC, Institute of Dentistry, University of Turku, Itäinen Pitkäkatu 4B (PharmaCity), 20520 Turku, Finland
[c] Department of Equine and Small Animal Medicine, Faculty of Veterinary Medicine, University of Helsinki, Helsinki, Finland

ARTICLE INFO

Keywords:
Composite implant
Contourable
Tailored fibre placement
Antebrachial fracture
Toy-breed dog

ABSTRACT

Fibre reinforced composites are attractive materials for hard tissue reconstructions, due to the high strength and low flexural modulus. However, lack of contourability in the operation theatre inhibits their clinical applications.

The study presents a novel *in situ* contourable composite implant system for load-bearing conditions. The implant system consists of a thin bioresorbable shell with several cavities, much like bubble-wrap. The central cavity contains a semi-flexible glass fibre preform prepared using Tailored Fibre Placement method. The preform is either pre-impregnated with a light curable resin, or the resin is injected into the cavity during the surgical procedure, followed by light curing. The semi-flexible glass fibre preforms were also examined as separate devices, "miniplates". Two types of miniplates were scrutinized, a simplified pilot design and a spatially refined, "optimized" design. The optimized miniplates were implemented as biostable and bioresorbable versions.

The feasibility of the *in situ* contourable composite implant system was demonstrated. The potential of Tailored Fibre Placement for the semi-flexible glass fibre preforms and miniplates was confirmed in a series of biomechanical tests. However, structural optimization is required. Antebrachial fractures in toy-breeds of dogs are exemplar veterinary applications of the devices; further applications in veterinary and human patients are foreseen.

1. Introduction

In this study, new concepts of composite fracture fixation devices were scrutinized. Antebrachial fractures in toy-breeds of dogs are exemplar veterinary applications of the devices, however, further applications in veterinary and human patients are foreseen. Antebrachial fractures, caused by even a minor impact, are particularly common in toy-breeds of dogs with body weights under 5 kg (Harasen, 2003; Muir, 1997). Fracture fixation with metallic plates is a typical treatment modality, however, the excessive stiffness of these devices may result in the adverse bone remodelling and complications in the healing of the fracture (Muroi et al., 2021).

Fibre reinforced composites (FRCs) are attractive material options for hard tissue reconstructions, as they have strength and lower flexural modulus comparable with those of their metallic counterparts (Evans and Gregson, 1998). A FRC fracture fixation plate with unidirectionally oriented reinforcing fibres is highly anisotropic and has the highest flexural strength orthogonal to the fibres but has low strength in torsion. A laminated structure with layers of fibres placed at an angle is a typical solution to this problem. However, both types of plate design have intrinsic drawbacks in clinical settings. Drilling screw holes through fibre layers exposes the fibre ends to the abrasive interaction with the typically metallic screws possibly resulting in the formation of metallic and ceramic debris and to consequent inflammation of the surrounding tissues (NEWBONE, 2010). Moreover, the holes disrupt the integrity of the reinforcement fibres and hence, the strength of the device (Moritz et al., 2016).

The structure of the plate can be enhanced by means of Tailored Fibre Placement (TFP) (Mattheij et al., 1998). In TFP, a textile additive manufacturing method, continuous fibre rovings are selectively placed onto a fabric sheet and fixed by stitching to prepare a reinforcing preform that can be refined into FRCs for a variety of applications (Rentsch

* Corresponding author at: Biomedical Engineering Research Group, Biomaterials and Medical Device Research Program, Itäinen Pitkäkatu 4B (PharmaCity), 20520 Turku, Finland.
E-mail address: julia.kulkova@utu.fi (J. Kulkova).

https://doi.org/10.1016/j.rvsc.2023.02.001
Received 21 February 2022; Received in revised form 31 October 2022; Accepted 6 February 2023
Available online 9 February 2023

et al., 2010; Hoyer et al., 2014; Rentsch et al., 2014; Breier, 2015; Hahner et al., 2015a; Hahner et al., 2015b;). In TFP, the fibre rovings can be placed according to the directions of the maximum stresses (Gliesche et al., 2003). Consequently, the stresses are uniformly distributed within the structure avoiding apparent stress concentrations. Moreover, the reinforcement fibres are placed to provide desired mechanical characteristics under the load, *e.g.* stiffness or acceptable degree of deformation in a particular direction. As another benefit of TFP technique, the reinforcement fibres can be localized to the areas where the reinforcement is actually needed keeping the device compact and lightweight. In addition, the reinforcement fibres bypass screw holes, but at the same time, the fibres are evenly distributed under the screw heads to ensure stable fixation of the devices. Thus, the integrity of the structure is not compromised and the abrasive interface between the screw and the composite is avoided.

Nevertheless, regardless of all the benefits of composites over metals and regardless of the optimal fibre placement within a composite fracture fixation device, there is a fundamental unsolved problem related to composites which inhibits their clinical application, namely, the contourability of the device. In many clinical applications, the surgeon would like to contour the fracture fixation device to the shape of the bone, which is typically irregular. Unlike the malleable metal counterparts, composite devices fail to fulfil this requirement. Consequently, there is a need to develop composite implants which are *in situ* contourable.

The primary aim of this study was to scrutinize an *in situ* contourable composite implant system applicable in load-bearing conditions. Thereafter, the reinforcing components of the system were examined as separate devices, "miniplates". Two types of TFP structures were scrutinized, a simplified pilot design, and a spatially refined, "optimized" design. Finite element (FE) analysis was employed to create spatially optimized TFP patterns with isoelastic behaviour. The miniplates with the spatially optimized TFP pattern were implemented as biostable and bioresorbable versions. The biostable FRC devices consisted of dimethacrylate-based polymer matrix reinforced with *E*-glass fibres.

The bioresorbable version was developed to aid the development of a completely bioresorbable *in-situ* contourable composite implant system described in our previous study (Plyusnin et al., 2021). A device with the optimized TFP pattern was prepared from polylactide matrix and hybrid yarn of polylactide (PLA) and glass fibres. In the future studies, these materials are expected to be substituted by completely bioresorbable counterparts (Plyusnin et al., 2021; Eichhorn et al., 2021).

2. Materials and methods

2.1. Clinical concept and methodology

Clinically used fracture fixation plates are either countered to the shape of bone before their attachment with screws, or have threaded holes for the attachment with locking screws. With metals, both options are easily achievable. With composites, however, both options are technically challenging. Contouring of composite implants is a particular challenge, as composite implants are typically pre-shaped and cannot be further bent or twisted. To tackle this challenge, we propose a novel type of *in-situ* contourable composite implant system shown in Fig. 1 (Kulkova, 2017).

The *in-situ* contourable composite implant system has two main functions: first, it acts as a traditional bone plate, fixing the bone in place to ensure fracture healing. Second, it delivers therapeutics to the fracture site. On the conceptual level, the implant system consists of a thin bioresorbable shell with several cavities, much like bubble-wrap. Each cavity has a specific content to serve a specific function. The central cavity contains a semi-flexible glass fibre preform. The semi-flexible glass fibre preform is either pre-impregnated with a light curable resin, or the resin is injected into the cavity containing the semi-flexible glass fibre preform during the surgical procedure. In turn, the lateral cavities could be loaded with silica-based bioactive glass (BG) granules to promote bone growth (Hoppe et al., 2011; Lindfors et al., 2010a) and prevent bacterial infections (Munukka et al., 2008; Lindfors et al., 2010b).

During the operation, the surgeon would position the *in-situ* contourable composite implant system onto the bone, contour the semi-flexible glass fibre preform to the bone, fix the *in-situ* contourable composite implant system with screws and then expose it to a typical dental blue light source that would cure the resin, creating a rigid fixture. The lateral cavities could be wrapped around the bone fracture to stimulate the healing process.

2.1.1. Semi-flexible glass fibre preform

The semi-flexible glass fibre preform prepared by TFP method is the backbone of the device. Initially, the semi-flexible glass fibre preform is flexible, but when completely cured, it becomes rigid and acts as a fracture fixation plate. In this study, the filling patterns for selective fibre placement within the semi-flexible glass fibre preforms were selected to take full advantage of the TFP technology and the biomechanics of fracture fixation plates (Fig. 2). The number of the strands of rovings in the filling pattern was minimized, since any end of a roving is considered as a potential stress concentrator or a seed of fibre/matrix debonding. Preferably, the filling pattern should be formed from one continuous strand of fibre roving.

From the functional standpoint, the rovings in the filling pattern are conceptually subdivided into segments of three main types: primary reinforcing segments, secondary reinforcing segments and contouring segments (Fig. 3).

Primary reinforcing segments are placed to match the directions of the main tensile stresses occurring within the device in the loaded state.

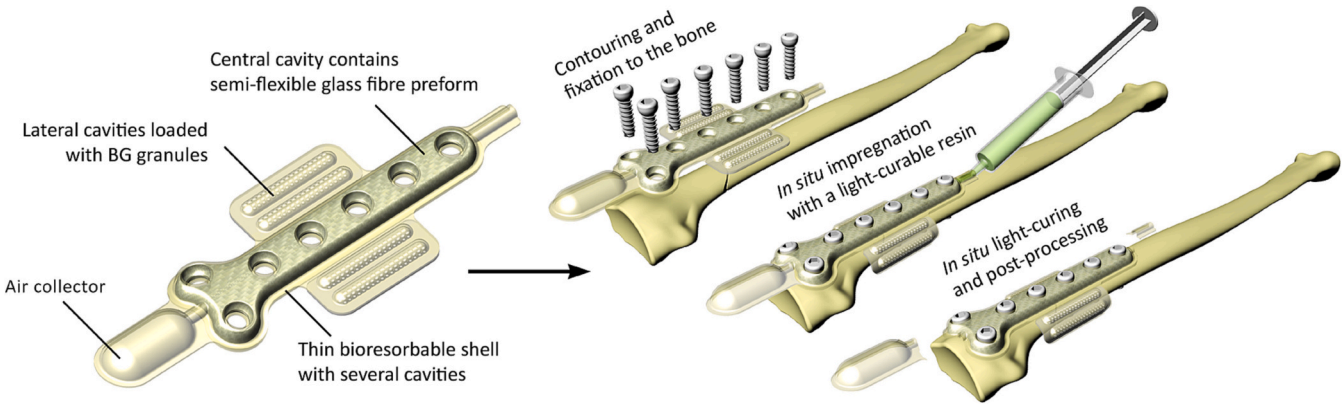

Fig. 1. Conceptual illustration of the novel type of *in-situ* contourable composite implant system.

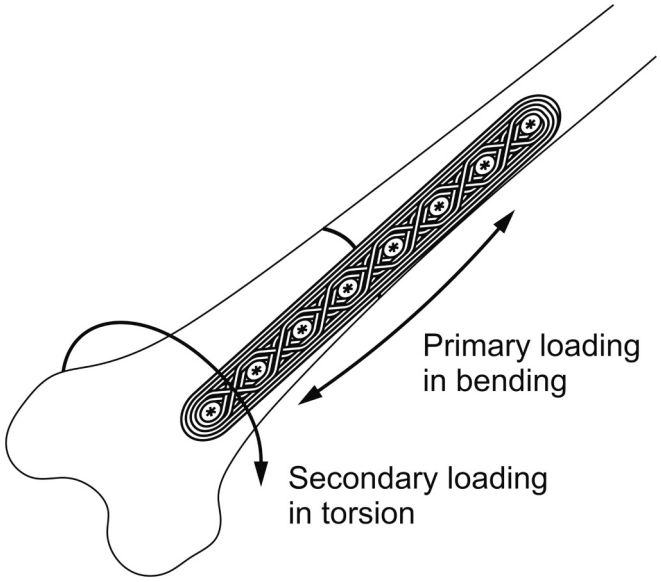

Fig. 2. Forces acting upon a load-bearing fixation plate: primary loading in bending and secondary loading in torsion.

In the case of a fracture fixation plate, bending is the primary loading mode and the device is primarily reinforced against bending by placing the segments in the direction of bending. Secondary reinforcing segments are placed along the maximum tensile stresses occurring in the second most probable loaded state; or along second principle stresses in the main loaded state. In the case of a fracture fixation plate, torsion is the secondary loading mode.

Contouring segments surround the whole filling pattern from outside and inside, including inner cut-offs *e.g.* screw holes, to provide additional structural integrity to the reinforcement phase and prevent, *e.g.*, tearing of the structure or avulsion of the screws.

This conceptual subdivision of the filling pattern into segments allows the description of the device in plain terms to aid the process of the structural and biomechanical optimization of the device. However, any of the segments may have one or more of the functions simultaneously. For example, a contouring segment placed in the direction of the first principle stress will also work as a primary reinforcing segment.

In this study, we have progressed from manufacturing and pilot testing of a prototype of the *in-situ* contourable composite implant system which contained a semi-flexible glass fibre preform prepared by TFP (1) towards spatial optimization and testing of the semi-flexible glass fibre preforms as separate devices (2). The spatial optimization was aimed at the creation of a functional device with uniform thickness without zones of non-reinforced matrix, however retaining the acceptable mechanical strength. The design of the study is shown in Fig. 4.

2.2. Manufacturing and pilot testing of a prototype of the in situ contourable composite implant system

The prototypes of the *in-situ* contourable composite implant system comprised a vacuum formed shell and a semi-flexible glass fibre prepreg encased within the shell. The semi-flexible glass fibre prepregs were prepared from the semi-flexible glass fibre preform impregnated in the light-curable resin matrix.

The semi-flexible glass fibre preform had a length of 35.5 mm, width of 5.5 mm and thickness of 1.5 mm and curvature with radius of 14 mm as shown in Fig. 5. The semi-flexible glass fibre preform had six screw holes with the distance between midpoints of adjacent screw holes being 6.0 mm. This design of the semi-flexible glass fibre preform is designated as pilot TFP (PTFP) preforms. The design of the fibre layout, as well as the fabrication of the PTFP preforms were performed in collaboration with TraceRay Oy, Turku, Finland and Biontec Bionic Composite Technologies AG, St Gallen, Switzerland. The PTFP preforms were prepared using rovings of *E*-glass fibres with the tex number of 600 (Ahlstrom Glassfibre Oy, Finland).

The PTFP preforms were then pre-impregnated with a photo curable resin matrix consisting of bisphenol A dimethacrylate and triethylene glycol dimethacrylate (BisGMA/TEGDMA) copolymers with respective mass percentages of 60 wt% and 40 wt%. Photoinitiator-activator system applied in polymerization of the resin consisted of camphorquinone (0.7 wt%) and dimethylaminoethyl methacrylate (DMAEMA) (0.7 wt%). Materials used in the study are listed in Table 1. The PTFP prepregs were then encased in the prefabricated shells of the *in situ* contourable composite implant system. The shell of the *in situ* contourable composite implant system, shown in Fig. 6, was designed and manufactured in collaboration with TraceRay Oy, Turku, Finland and Medical Advanced Manufacturing Research Centre (AMRC), the University of Sheffield, UK. Polycarbonate forming was used as a surrogate for the bioresorbable polymer. The forming was prepared by a vacuum forming method developed specifically for the purpose. To ensure the relevance of the forming method, it was tested with Poly(DL-lactide-*co*-glycolide) (PDLGA), a commercially available medical grade bioresorbable polymer (Zeus Industrial Products Ltd., Ireland), the target material for the shell of the *in situ* contourable composite implant system (Fig. 6A).

Three groups of specimens were fabricated: unreinforced miniplate-shaped BisGMA/TEGDMA resin specimens ($N = 6$), cured in moulds, miniplate-shaped reinforced specimens made of PTFP prepregs ($N = 3$),

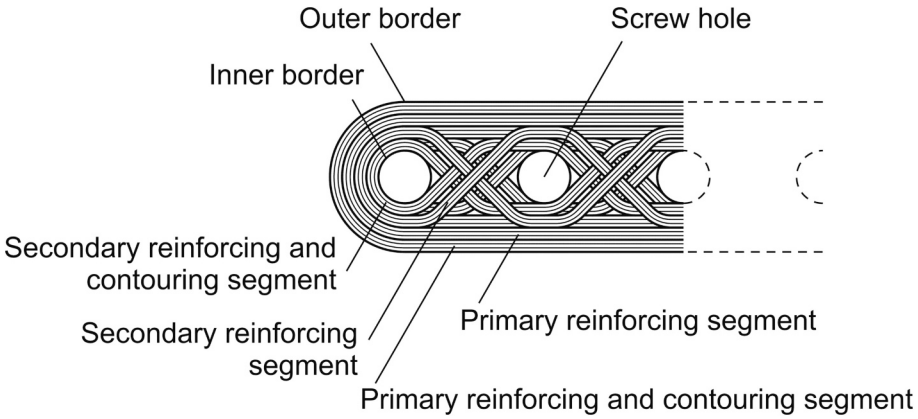

Fig. 3. A load bearing device with an outer border, an inner border and screw holes. Respective functionalized placement of a continuous roving in the device: primary reinforcing segment, segment with combined primary reinforcing and contouring functions, secondary reinforcing segment and segment with combined secondary reinforcing and contouring functions.

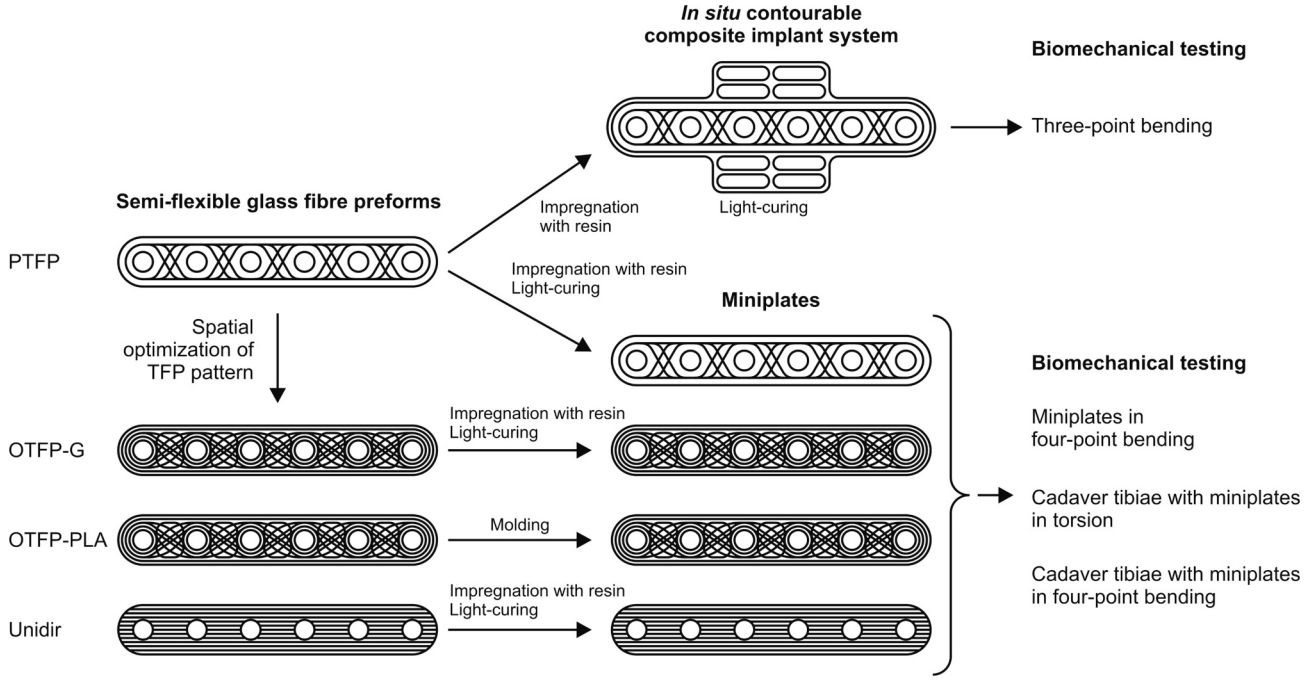

Fig. 4. Schematic illustration of the design of the study. Acronyms: PTFP = Pilot TFP pattern, OTFP-G = TFP pattern with the spatial optimization within BisGMA/TEGDMA matrix, OTFP-G = TFP pattern with the spatial optimization within PLA matrix Unidir = BisGMA/TEGDMA matrix reinforced with unidirectional fibres.

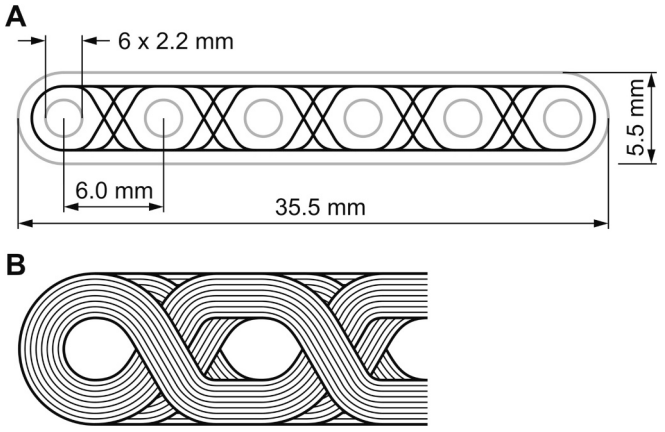

Fig. 5. The dimensions and TFP patterns used in the PTFP preforms and respective miniplates. A) Black tracings represent the central lines of the rovings. The outlines of the plates and holes are shown in grey colour. B) Schematic illustration of the actual placement of the rovings within the plate.

and reinforced specimens made of PTFP prepregs encased in the polycarbonate shell ($N = 5$). All specimens were cured by a blue light curer similar to that intended for use in operation theatre, with an irradiance of 1200 mW/cm^2 for 40 s. The curing was considered relevant for the clinical settings.

Three-point bending tests were performed on the three groups of specimens. The rollers within the three-point bending test jig were positioned such that the load was applied between the two central screw holes, and between the two outermost screw holes. The roller to roller distance equalled 24 mm. The testing was performed on a universal testing machine (Shimadzu Corporation, Kyoto, Japan), utilizing a sensitive 10 kN load cell to ensure the expected low force values were detected. A pre-load of 0.2 N and a velocity of 1 mm/min were used for all specimens.

Table 1
Materials used in the study.

Material	Type of material	Manufacturer
Bisphenol-A-glycidylmethacrylate (BisGMA)	Comonomer	Röhm Chemische Fabrik GmbH, Darmstadt, Germany
Triethylene glycol dimethacrylate (TEGDMA)	Comonomer	Aldrich Chemie GmbH, Steinheim, Germany
Camphorquinone	Photoinitiator	Sigma-Aldrich GmbH, Buchs, Switzerland
Dimethylaminoethyl methacrylate (DMAEMA)	Activator	Fluka Chemie GmbH, Buchs, Switzerland
Poly(DL-lactide-co-glycolide) (PDLGA)	Bioresorbable polymer	Zeus Industrial Products (Ireland) Ltd.
Polylactide (PLA)	Bioresorbable polymer	Trevira GmbH, Bobingen, Germany
R338	*E*-glass fibre	Ahlstrom Glassfibre Oy, Kotka, Finland
EC14 300 TD44C	E-glass fibre	Saint-Gobain Vetrotex, Aachen, Germany

2.3. Spatial optimization and testing of the semi-flexible glass fibre preform implemented as miniplates

In this phase of the study, we have scrutinized the mechanical properties of the completely cured prepregs with the perspective of using them as parts of the *in-situ* contourable composite implant system and as such, as miniplates for the fixation of bone fractures in human and animal patients.

A series of mechanical testing was performed to assess the mechanical performance of the miniplates. The mechanical tests included testing of the miniplates as such as well as in conjunction with bones to simulate the fixation of bone fractures.

2.3.1. Spatial optimization

The models applied in FE simulations were engineered according to the corresponding physical mechanical test modalities. A commercial computer aided engineering programme Abaqus/Standard 2017 (Dassault Systemes Simulia Corp., USA) was utilized. Identical two-

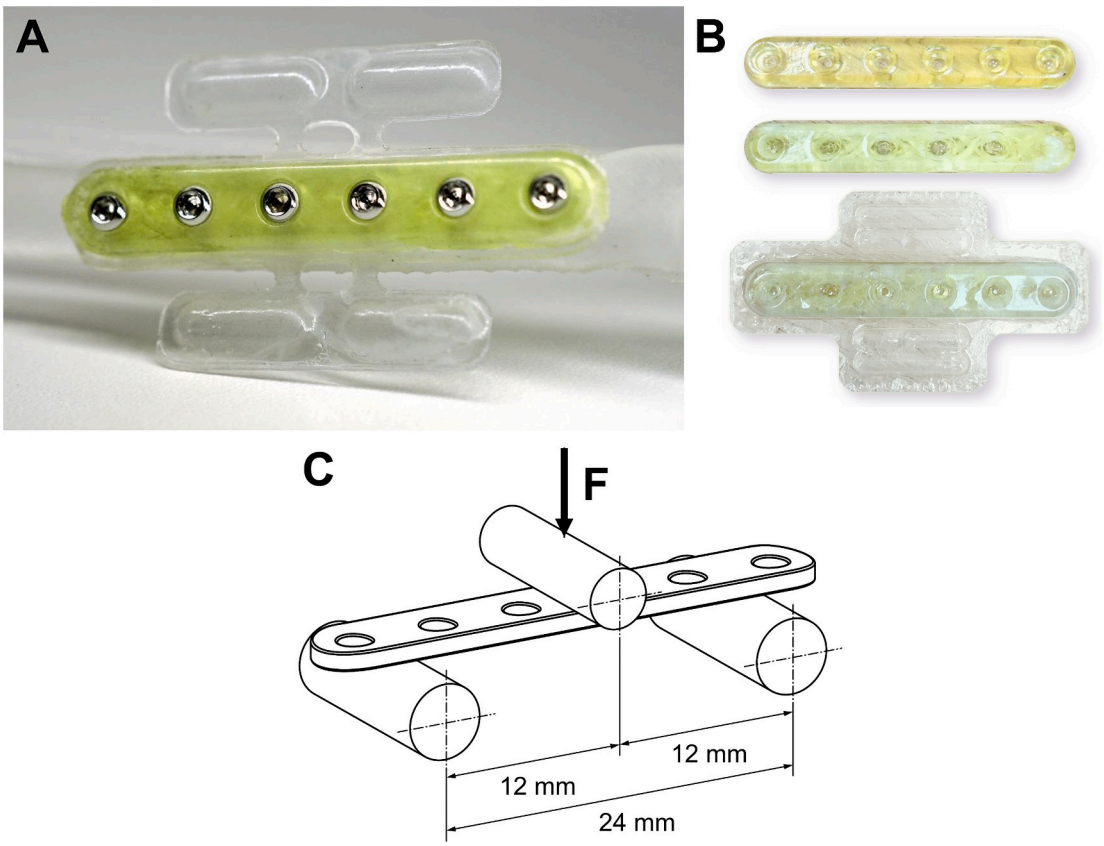

Fig. 6. A) The ultimate technical implementation of the prototype of the novel type of *in situ* contourable composite implant system comprising a shell made of PDLGA and PTFP prepreg. B) Specimens used in the study (from top to bottom): unreinforced resin specimens, reinforced specimens made of PTFP prepreg and specimens made of PTFP prepreg encased in the polycarbonate shell. C) Schematic illustration of the three-point bending test setup.

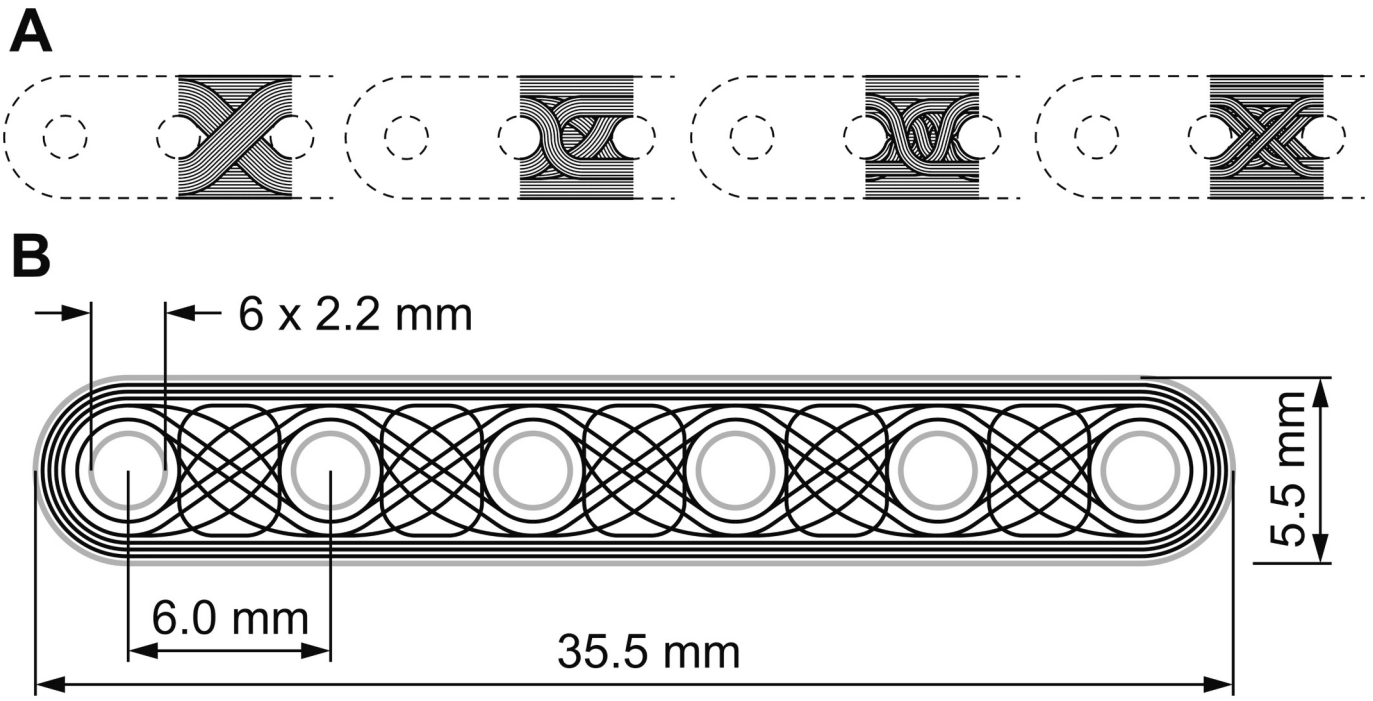

Fig. 7. A) The principles of spatial optimization of the structure achieved by using rovings with lower tex number while maintaining the same overall number of reinforcing fibres applied in this study. B) The ultimate design for TFP patterns used in the OTFP preforms and respective miniplates. Black tracings represent the central lines of the rovings. The outlines of the plates and holes are shown in grey colour.

dimensional finite element mesh was used for all miniplate designs. The two-dimensional pattern was then applied to each layer in the third dimension. Due to varying fibre alignments, the total number of elements was different in each miniplate design. In Unidir miniplates, thickness of the layers was set to correspond to the horizontal dimension of the elements. In TFP miniplates, the meshes were generated utilizing a meshing software package (AOPS, IPF Dresden, Germany). In this approach, each fibre roving loop was represented by a separate layer of elements whose thickness was determined by Tex number of the fibres and fibre volume content.

All the simulations were performed as general static problems. The element type for all miniplates was C3D8. Values of mechanical quantities describing resin and fibre properties were taken from literature. The bones were modelled as elastic bodies. The element type utilized was C3D8. In all simulations, the screws were modelled as rigid bodies. The osteotomy site was modelled as hard frictionless contact without a gap.

In four-point bending simulations, loading and support noses were modelled as rigid bodies. The element types applied were rigid tri- and quadrilateral 3D elements (R3D3 and R3D4). No movement of the supports was allowed, and the loading noses could move in a vertical plane only. In the simulation of the miniplates, a total concentrated force of 100 N was directed through the loading noses. In the simulation of the constructs consisting of tibiae joined with miniplates, the corresponding force was 200 N. Interactions between the testing specimens and loading and support noses were modelled as hard contacts with friction coefficient of 0.05. In the torsion test, one end of the construct was fixed in all directions. In respect to the point lying on the construct's longitudinal central axis at the other end, torque of 1 N·m was applied.

Spatial optimization of the miniplate design was done as an iterative process (Fig. 7). Based on the simulation of mechanical tests, changes to the existing FE mesh representing the loops of the fibre rovings within the miniplate were made. Consequently, a new simulation was conducted. The final design, selected for manufacturing of the physical specimens, was empirically derived from the intermediate simulated designs, in which one of the types of rovings (primary, secondary reinforcing segments or contouring segments, including those forming the screw holes) was prevailing to estimate the effect of these or that changes. Nine rounds of iteration were run prior to achieving the TFP pattern applied for producing the optimized TFP miniplates.

The tasks of the optimization process were to achieve acceptable values of structural stiffness, optimize the fibre volume distribution to provide uniform thickness of the miniplate, and reduce the critically loaded volume fraction within the miniplate. Moreover, the proximity of the holes was aimed to reinforce the mechanical strain resulting from the screws. As for their contribution to the overall mechanical performance of the miniplate, the rovings were subdivided into three groups. Fibres oriented along the longitudinal axis of the miniplate were expected to give rise to flexural strength of the miniplate. These fibres were located at the edges of the miniplate. The overlapping fibres at the areas between the holes were intended to contribute to torsion resistance of the miniplate. The fibre loops around the holes were expected to give resistance to the strain caused by the screws.

2.3.2. Biomechanical testing of miniplates

Altogether, four groups of miniplates with the same geometrical dimensions as described in Section 2.2 were prepared for the study (Table 2):

Group Unidir comprised control miniplates made of BisGMA/TEGDMA resin matrix reinforced with continuous unidirectional *E*-glass fibres. The reinforcement contained E-glass fibres with diameter of 15 μm and tex number of 2400 (R338–2400, Ahlstrom Glassfibre Oy, Finland). To achieve the aimed volume fraction of 0.5, five fibre rovings were mixed with corresponding amounts of resin. These miniplates served as a control group (Liesmäki et al., 2019).

Group PTFP comprised miniplates of BisGMA/TEGDMA resin matrix reinforced with PTFP preforms. The preforms were identical to those used in the *in situ* contourable composite implant system described earlier in the text.

Group OTFP-G comprised miniplates of BisGMA/TEGDMA resin matrix reinforced with preforms manufactured by TFP with the spatial optimization. For TFP plates with optimized fibre pattern, *E*-glass fibres with and tex number of 300 (EC14 300 TD44C, Saint-Gobain Vetrotex, Aachen, Germany) were used. Preforms from both PTFP and OTFP-G groups were also impregnated with the amount of resin resulting in volume fraction of 0.5 as in the case of Unidir group.

The manufacturing process for miniplates in groups Unidir, PTFP and OTFP-G with BisGMA/TEGDMA resin matrix reinforced E-glass fibres followed the same protocol. Fibre volume content was 0.5 for all plate designs. The glass fibre preforms were impregnated with the BisGMA/TEGDMA resin matrix in a heat cabinet (BE600, Memmert GmbH + Co. KG, Germany) at 39 °C for one hour. The resulting prepregs were transferred into individual moulds, wrapped in aluminium foil and set into a vacuum oven (VO400, Memmert GmbH + Co.KG, Germany) at atmosphere of 10 mbar and temperature of 25 °C for 38 min. to get rid of air pockets between fibres. The prepregs were thereafter covered with an additional layer of resin and pre-cured with a dental hand curing device (Elipar S10, 3 M ESPE, Seefeld, Germany) for 2 min. The specimens were then post-cured in a vacuum light oven (Visio Beta vario, 3 M ESPE, Seefeld, Germany) for 15 min. and in a light oven (Liculite, Dentsply De Trey GmbH, Dreieich, Germany) for 25 min. at ambient temperature.

Group OTFP-PLA comprised miniplates fabricated using the same TFP pattern as OTFP-G but prepared of PLA-*E*-glass hybrid yarns and PLA as a matrix material. A hybrid yarn containing one roving of 300 tex E-glass fibres and 16 rovings of 167 dTex (decitex) PLA was utilized in production of preforms for miniplates with PLA matrix. The preforms for miniplates with PLA matrix were embroidered according to the optimized fibre pattern on a PLA film with thickness of 0.2 mm.

The miniplates in OTFP-PLA were produced by hot pressing in a two-piece mould made of aluminium alloy. Before hot pressing, the preforms were dried for three hours at 80 °C. Consequently, the preforms were transferred into the mould and to a hot press machine. Air from the working zone of the hot press was deflated to 50 mbar and the mould

Table 2
Summary of the tested specimens.

Group	Matrix	Reinforcement phase	Number of miniplates tested in four-point bending	Number of constructs tested in torsion	Number of constructs tested in four-point bending
Unidir	BisGMA/TEGDMA (60/40)	Continuous unidirectional E-glass fibres	5	5	5
PTFP	BisGMA/TEGDMA (60/40)	Continuous unidirectional E-glass fibres	5	5	5
OTFP-G	BisGMA/TEGDMA (60/40)	Continuous unidirectional E-glass fibres	5	5	5
OTFP-PLA	PLA		5	5	5
Intact chicken tibia				9	7

was exposed with pressure of 8 bar. Temperature of the working surface was incrementally risen to 200 °C at the rate of 15 °C/min after which the pressure was increased to 10 bar. After maintaining the temperature of 200 °C for five minutes, the mould was let to cool down to 25 °C within two hours. Consequently, pressure of the mould and vacuum of the working surface were released, and the miniplates were collected.

2.3.3. Preparation of cadaver tibiae for mechanical testing

The bone samples utilized in this study were chicken tibiae extracted from commercially available chicken drumsticks from four Finnish producers of Atria company (330, A. ja V. Rantala farm, Atria). Chicken tibias were selected as a substitution for toy-breed dog's radius due to similar dimensions and availability. The soft tissues along with epiphyseal cartilage were removed by hand and the bones were stored in a refrigerator at 8 °C wrapped in wet tissues. The bones were tested within 24 h after the extraction from soft tissues and were kept moisturized throughout the preparation and testing processes.

From the bones tested in four-point bending, proximal and distal ends were cut off at metaphyseal region with resulting bone length of 70 mm. Consequently, six screw holes with a diameter of 1.6 mm were drilled through the diaphyseal section of the bone and an osteotomy dividing the bone into two equally sized halves along its transverse axis was performed. The bone ends were joined with a miniplate placed on the anterior surface by means of six surgical screws with diameter of 2.0 mm and length of 12 mm (MF Cortex Screw, Synthes, Switzerland).

The bones that were tested in torsion were first embedded in polymethylmethacrylate (PMMA; Vertex Dental B.V., The Netherlands) in a special mould from their both ends. Prior to embedding, length of the bones was adjusted to 90 mm, resulting in a 70 mm span between the PMMA blocks. Thereafter, the screw holes were drilled, osteotomy performed and a miniplate attached in a similar manner as with the bones for the bending test.

In addition to the constructs of osteotomized bones joined with miniplates, a control group of bones was prepared for both mechanical testing methods. That is, the diaphyseal proportions remained intact with neither holes being screwed nor osteotomy being performed.

2.3.4. Mechanical testing of miniplates in four-point bending

The miniplates were tested in mechanical four-point bending according to the International Standard ISO 9585. Consequently, the load span k was set to 13.8 mm and the support span ($k + 2\ h$) to 27.6 mm. The radius of cylindrical shaped loading noses and supports (*D1* and *D2*, respectively) was 5.0 mm. A schematic illustration of a four-point bending setup is represented in Fig. 8.

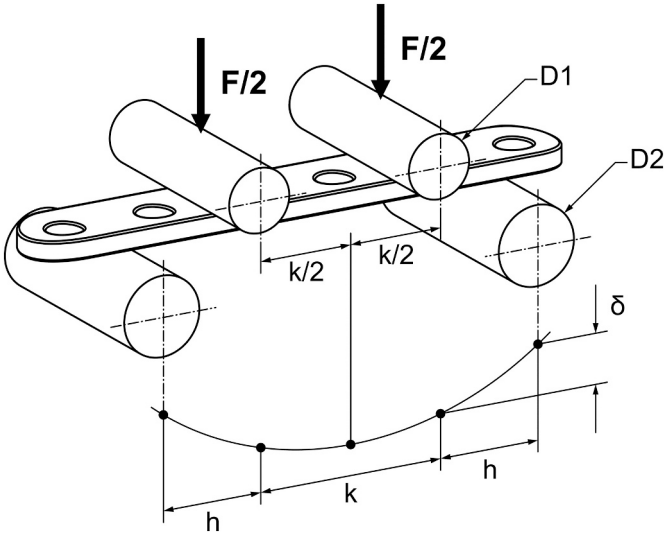

Fig. 8. A schematic illustration of a four-point bending test setup with relevant measures of length labelled.

A universal material testing machine (model LRX, Lloyd Instruments Ltd., Fareham, England) was utilized to produce loading velocity of 1.0 mm/min applied in posterior-anterior direction. The load-deflection curves were documented by means of commercial computer software (Nexygen, Lloyd Instruments Ltd., Fareham, England).

The measurement was continued until failure of the plate. Maximum loading F (N) and the slope of the linear region S (N/m) were determined from the load-deflection curves. Based on these quantities, the equivalent bending stiffness E (N·m^2) and bending strength B (N·m) of the plates were consequently derived for each group according to the formulas

$$E = \frac{(2h + 3k)Sh^2}{12}$$

and

$$B = 0.4Fh,$$

where E, h, k, and S are as determined above.

2.3.5. Mechanical testing of cadaver tibiae with miniplates in torsion

The constructs of osteotomized chicken bones fixed with miniplates were tested in torsion according to the setup utilized by Sod et al. (2005) with modifications due to different plate dimensions. A material testing machine (Avalon Technologies, Rochester, MI, USA) was utilized to produce a torsion rate of 64°/min applied in earlier studies with similar setup (Zhao et al., 2009). A torsion test in progress is represented in Fig. 9.

To mimic the physiological loading of tibia, the direction of torsional loading was determined so that the proximal end rotates externally in relation to the distal (Yang et al., 2014). The measurement was continued until failure of the bone or the plate, depending on which occurred first. Maximum torque τ (N·m) and angle of rotation α (deg, °) at failure were determined from the moment-angle curve. Based on these quantities, torsional stiffness S_τ (N·m/rad) of the constructs was consequently derived for each group according to the relation

$$S_\tau = \tau c/\alpha,$$

where c is the conversion coefficient yielding newton-metres per radian (180°/π) while S_τ, τ, and α are as above.

2.3.6. Mechanical testing of cadaver tibiae with miniplates in four-point bending

The constructs of osteotomized chicken bones fixed with miniplates were tested in mechanical four-point bending according to the setup utilized in (Sod et al., 2005) with modifications due to different plate dimensions. Hence, the load span was set to 27.6 mm and the support span to 55.2 mm. The radius of cylindrical shaped loading noses and supports was 5.0 mm. A universal material testing machine (model LRX, Lloyd Instruments Ltd., Fareham, England) was utilized to produce loading velocity of 1.0 mm/min applied in posterior-anterior direction. The load-deflection curves were documented utilizing a commercial computer software (Nexygen, Lloyd Instruments Ltd., Fareham, England). A construct tested in four-point bending is represented in Fig. 10.

The measurement was continued until failure of the bone or the plate, depending on which occurred first. Maximum loading F (N) and the slope of the linear region S (N/m) were determined from the load-deflection curves. Based on these quantities, the equivalent bending stiffness E (N·m^2) and bending strength B (N·m) of the constructs were consequently derived for each group.

2.3.7. Statistical analysis

Statistical analysis of the mechanical data was executed with a commercial computer software (SPSS Inc., Chicago, Illinois, USA). Normality of the data was tested with Kolmogorov-Smirnov test and

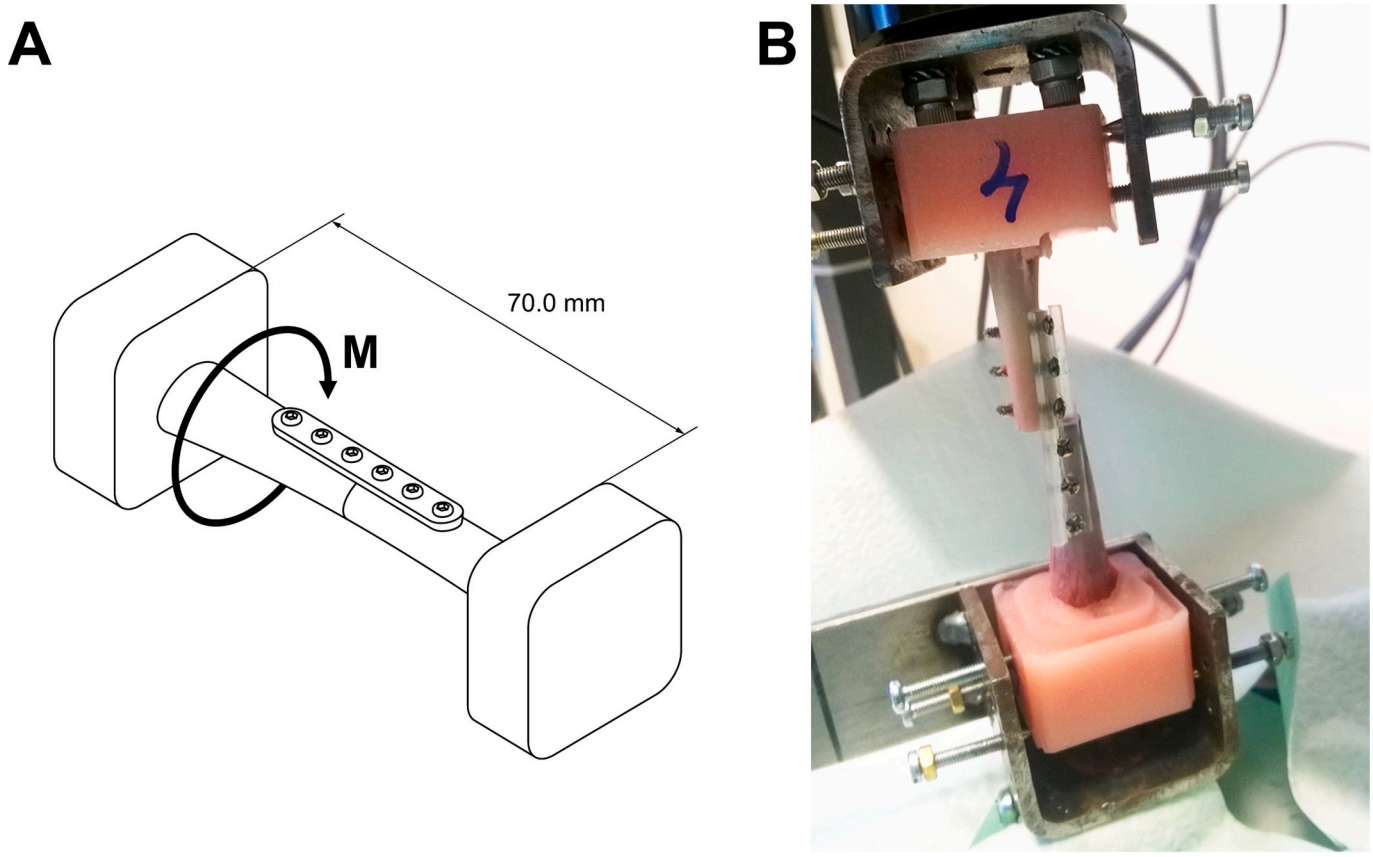

Fig. 9. A) Schematic illustration of the torsion test setup. B) A torsion test in progress.

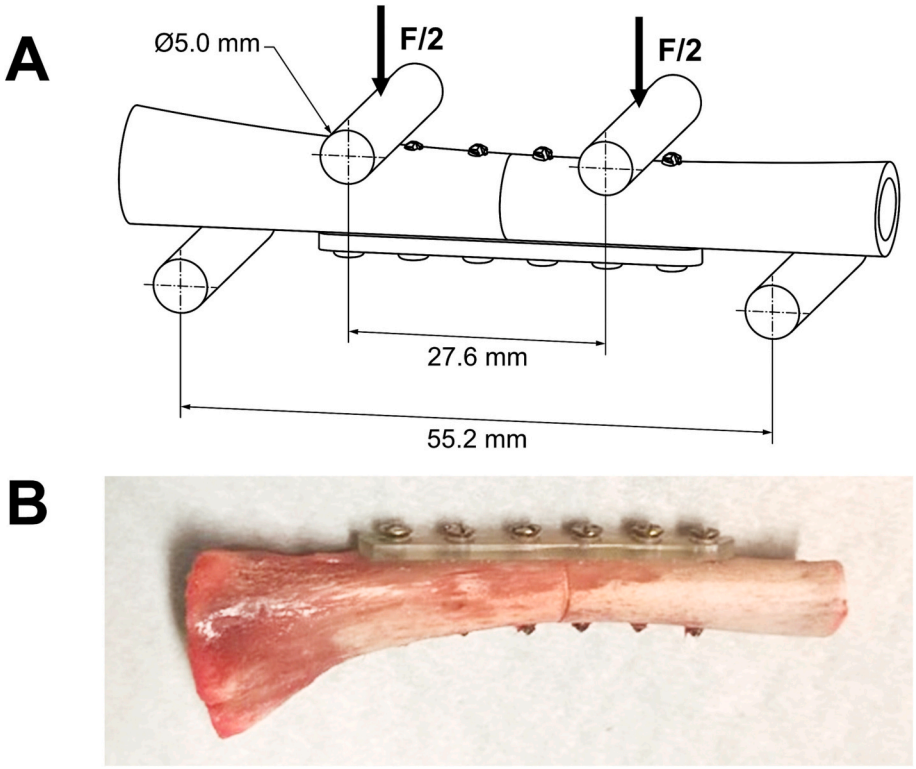

Fig. 10. A) Schematic illustration of the four-point bending test setup. B) A construct tested in four-point bending.

homogeneity of variances with Levene's test. For normally distributed data groups with equal variances, one-way ANOVA and consequent Tuckey's *post hoc t*-tests were applied while comparing the groups. In the case of non-normal data distribution or unequal variances, Kruskal-Wallis test and consequent *post hoc* Mann-Whitney *U* tests were performed. The considered level of statistical significance was 0.05.

3. Results

3.1. Manufacturing and pilot testing of a prototype of the in situ contourable composite implant system

The various prototype iterations of the *in situ* contourable composite implant system have systematically addressed issues within the proposed manufacturing and assembly method.

The three-point bending tests indicated that the PTFP reinforcement did increase the strength of the bone plate. The ultimate load values (expressed as mean ± standard deviation) obtained from force-displacement curves were 46.8 ± 13.0 N for the unreinforced resin specimens, 107.5 ± 29.2 N for the reinforced specimens made of PTFP and 177.8 ± 70.7 N for the PTFP prepregs encased in the shells. The lowest failure point for the reinforced specimens made of PTFP, 75.15 N, was similar to the highest failure point for the unreinforced resin specimens, 71.28 N. However, the unreinforced resin specimens were over filled, and screw holes were closed off with the excess resin. Aside from the apparent increase in overall strength, the PTFP prepregs encased in the shells were also able to withstand higher forces following the initial failure. It was also demonstrated that the *in situ* contourable composite implant system would remain as a single piece after the maximum force had been achieved and the load rating gradually decreased.

3.2. Biomechanical testing of the miniplates

3.2.1. Biomechanical testing of miniplates in four-point bending

The results of the mechanical testing of the miniplates in four-point bending are presented in Fig. 11 and Table 3.

In respect of each studied parameter, Kolmogorov-Smirnov test confirmed the data to be normally distributed. Requirement of equal variances was met in slope and equivalent bending stiffness. One-way ANOVA and consequent Tuckey's *post hoc t*-test was applied in comparison of the groups in respect of these parameters. Due to unequal variances, distributions of maximum load and bending strength were assessed by Kruskal-Wallis test and consequent *post hoc* Mann-Whitney pairwise comparisons.

Maximum load in group Unidir was statistically significantly greater than that in any other group ($P = 0.008$). Maximum load in group OTFP-G was statistically significantly lower than that in groups PTFP and OTFP-G ($P = 0.016$ and $P = 0.047$, respectively). There were no other statistically significant differences in maximum load.

In group Unidir, the slope of the load-deflection curve was statistically significantly greater than that in any other group ($P < 0.001$). Slope of the group OTFP-PLA was statistically significantly greater than that in groups OTFP-G and PTFP ($P < 0.001$ and $P = 0.044$, respectively). There were no other statistically significant differences in slope.

Equivalent bending stiffness of the group Unidir was statistically significantly higher than that in any other group ($P < 0.001$). Equivalent bending stiffness of the group OTFP-PLA was statistically significantly higher than that in groups OTFP-G and PTFP ($P < 0.001$ and $P = 0.044$,

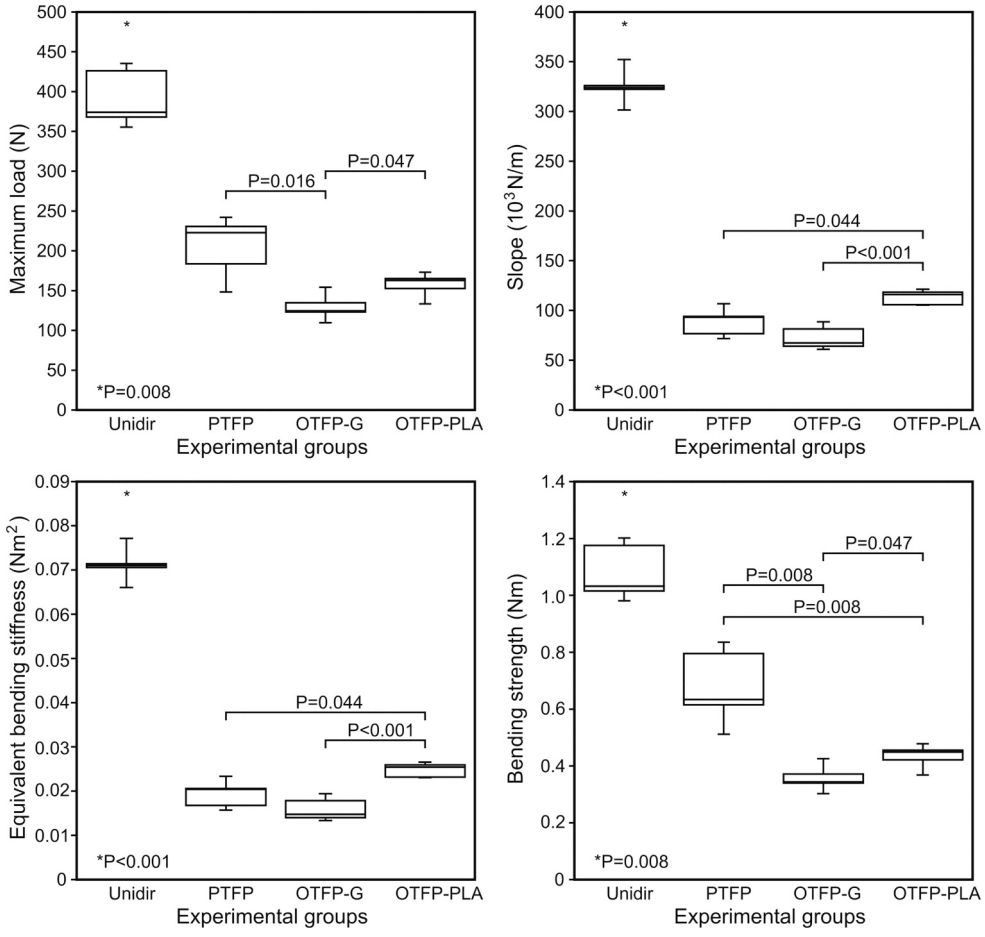

Fig. 11. Boxplots for maximum load, slope, equivalent bending stiffness, and bending strength of the miniplates assessed in the four-point bending.

Table 3
Results of the biomechanical testing of miniplates.

Parameter	Group				
	Unidir	PTFP	OTFP-G	OTFP-PLA	Chicken tibia as such
Four-point bending test of miniplates					
Maximum load *F*, N [b]	373.9 (368.0, 426.1)	222.8 (183.8, 230.5)	124.6 (123.2, 134.7)	162.7 (152.7, 165.1)	
Slope *S*, N/m [a]	325.2 ± 18.1	88.4 ± 14.2	72.4 ± 12.0	113.4 ± 7.4	
Equivalent bending stiffness *E*, N·m^2 [a]	0.071 ± 0.004	0.019 ± 0.003	0.016 ± 0.003	0.025 ± 0.002	
Bending strength *B*, N·m [b]	1.03 (1.02, 1.18)	0.63 (0.61, 0.80)	0.343 (0.340, 0.372)	0.45 (0.42, 0.46)	
Torsion test of constructs (cadaver tibiae fixed with miniplates)					
Maximum torque τ, N·m [a]	0.25 ± 0.08	0.54 ± 0.21	0.82 ± 0.23	0.91 ± 0.25	2.01 ± 0.37
Angle at τ α, degrees [b]	13.42 (9.48, 14.64)	24.12 (22.47, 31.10)	61.18 (26.73, 62.73)	40.58 (35.68, 44.09)	1.07 (1.04, 1.58)
Torsional stiffness S_t, N·m/rad [b]	1.07 (1.04, 1.58)	1.41 (1.06, 2.17)	1.51 (1.33, 2.46)	2.28 (2.25, 2.41)	13.80 (13.15, 18.80)
Four-point bending test of constructs (cadaver tibiae fixed with miniplates)					
Maximum load *F*, N [a]	225.8 ± 83.6	266.3 ± 30.4	262.4 ± 55.1	234.8 ± 79.8	308.3 ± 54.2
Slope *S*, N/m [a]	177.0 ± 31.0	135.1 ± 42.2	218.8 ± 62.5	180.8 ± 37.3	167.4 ± 43.6
Equivalent bending stiffness *E*, N·m^2 [a]	0.31 ± 0.05	0.24 ± 0.07	0.38 ± 0.11	0.32 ± 0.07	0.29 ± 0.08
Bending strength *B*, N·m [a]	1.25 ± 0.46	1.47 ± 0.17	1.45 ± 0.30	1.30 ± 0.44	1.70 ± 0.30

[a] Data presented as mean ± standard deviation.
[b] Data presented as median (1st, 3rd quartile).

respectively). There were no other statistically significant differences in the equivalent bending stiffness.

Bending strength in group Unidir was statistically significantly higher than that in any other group ($P = 0.008$) Bending strength in group PTFP was statistically significantly higher than that in groups OTFP-G and OTFP-PLA (P = 0.008 and P = 0.008). In group OTFP-PLA, bending strength was statistically significantly higher than that in group OTFP-G ($P = 0.047$). There were no other statistically significant differences in bending strength.

In bending tests of the miniplates, the miniplates with unidirectional reinforcement were observed to develop a crack propagating through the miniplate before the eventual material failure as shown in Fig. 12.

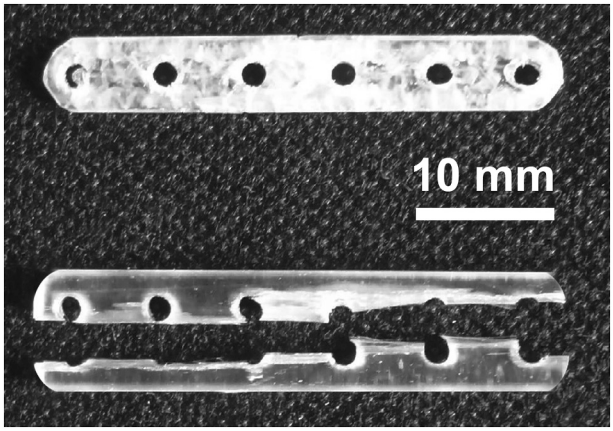

Fig. 12. Miniplates of PTFP and Unidir after the bending tests.

3.2.2. *Biomechanical testing of cadaver tibiae joined with miniplates in torsion*

Results of the mechanical testing of cadaver tibiae with plates in torsion are presented in Fig. 13 and Table 3.

In respect of each studied parameter, Kolmogorov-Smirnov test confirmed the data to be normally distributed. Requirement of equal variances was met in maximum torque. One-way ANOVA and consequent Tuckey's *post hoc t*-test was applied in comparison of the groups in respect of this parameter. Due to unequal variances, distributions of angle at maximum torque and torsional stiffness were assessed by Kruskal-Wallis test and consequent *post hoc* Mann-Whitney pairwise comparisons.

In groups OTFP-G and OTFP-PLA, the maximum torque resistance was statistically significantly higher than that of group Unidir ($P = 0.002$ and $P < 0.001$, respectively). In addition, maximum torque resistance was statistically significantly higher in the intact chicken tibia group than in any other group (P < 0.001). There were no other statistically significant differences in maximum torque.

In groups OTFP-G and OTFP-PLA, the angle at maximum torque was statistically significantly higher than that in group Unidir ($P = 0.008$ and P = 0.008, respectively). The angles at maximum torque in groups OTFP-G and OTFP-PLA were also statistically significantly higher than that in the intact chicken tibia group ($P = 0.001$ and $P = 0.007$, respectively). There were no other statistically significant differences in angle at maximum torque.

In group OTFP-PLA, torsional stiffness was statistically significantly higher than that in group Unidir ($P = 0.016$). Torsional stiffness of the group intact chicken tibia was also statistically significantly higher than that in any other group (P = 0.001). There were no other statistically significant differences in torsional stiffness.

3.2.3. *Biomechanical testing of cadaver tibiae joined with miniplates in four-point bending*

Results of the Mechanical testing of cadaver tibiae with miniplates in four-point bending are shown in Fig. 14 and Table 3.

In respect of each studied parameter, Kolmogorov-Smirnov test confirmed the data to be normally distributed. Requirement of equal variances was met in every parameter. One-way ANOVA and consequent Tuckey's *post hoc t*-test was applied in comparison of the groups.

No statistically significant differences between the groups were observed in four-point bending of the constructs in respect of any measured parameter.

4. Discussion

The study has demonstrated a proof-of-concept of a novel type of *in situ* contourable composite implant system proposed earlier [Kulkova, 2017; Plyusnin et al., 2021). The *in situ* contourable composite implant system was possible to implement technically and it was capable of withstanding substantial mechanical loads without disintegration. In addition, the study has addressed the task of application of TFP technology for the fabrication of the reinforcement element of the *in situ* contourable composite implant system. Moreover, a structural optimization of the TFP patterns and utilization of the reinforcement element of the *in situ* contourable composite implant system *per se*, as a separate load-sharing fracture fixation device was scrutinized in biostable and bioresorbable forms.

FRCs have been successfully utilized in various clinical applications (Karmaker et al., 1997; Evans and Gregson, 1998; Vallittu, 1999; Ramakrishna et al., 2001; Vallittu, 2017). This is due to their tailorability to promote isoelastic properties with cortical bone along with good biocompatibility and osseointegration (Tuusa et al., 2007; Tuusa et al., 2008; Zhao et al., 2009; Aitasalo et al., 2014; Moritz et al., 2014;

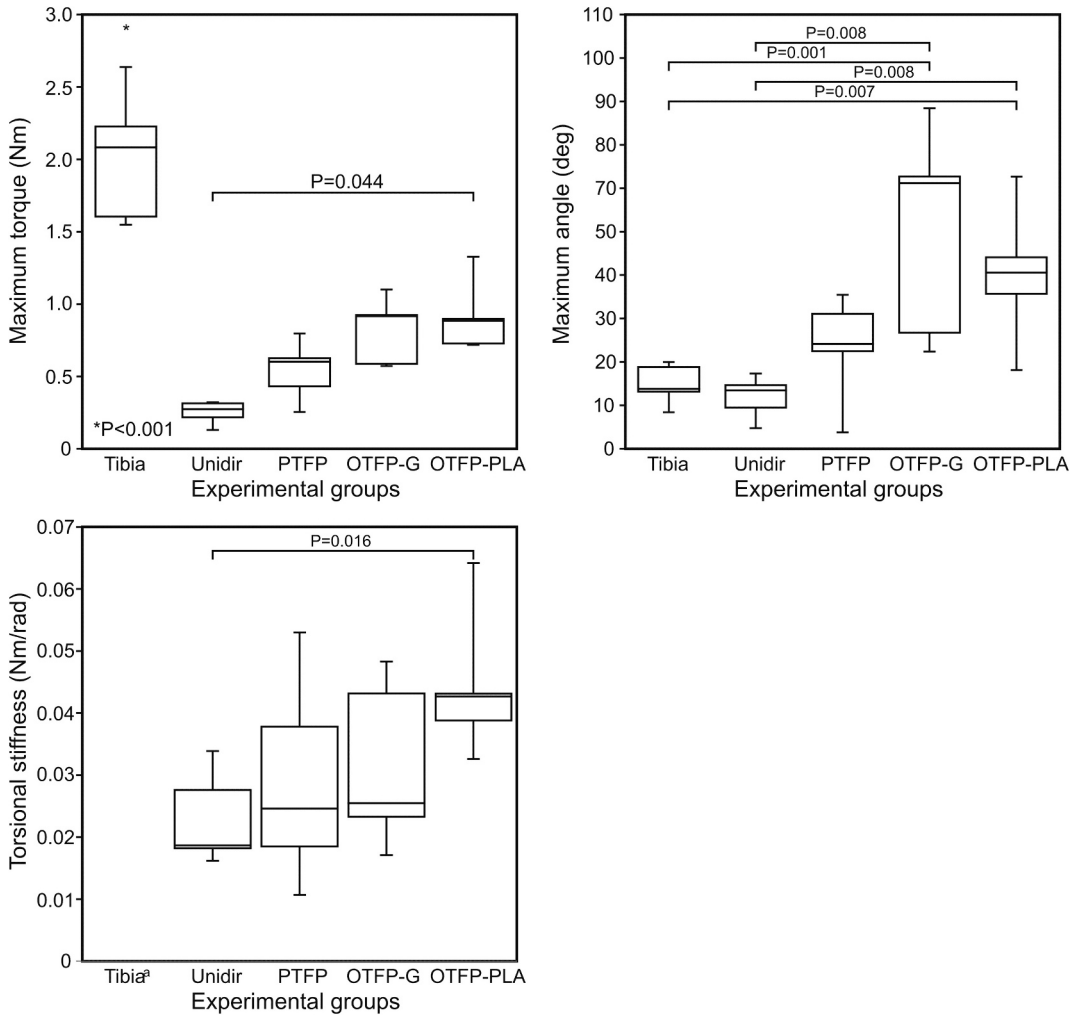

Fig. 13. Boxplots for maximum torque, angle of rotation at maximum torque, and torsional stiffness of the constructs assessed in the four-point bending. [a] Group intact chicken tibia excluded from the boxplot (13.80 (13.15, 18.80) N·m/rad, $P = 0.001$).

Piitulainen et al., 2015). Both biostable and bioresorbable material candidates have been proven to be suitable for load bearing FRC-based devices (Saikku-Bäckström et al., 2000; Saikku-Bäckström et al., 2005; Aitasalo et al., 2014; Piitulainen et al., 2015). FRCs can be fabricated into highly anisotropic material compositions with high load bearing capacity (Zhao et al., 2009; Moritz et al., 2014; Moritz et al., 2016).

The growing market of implantable medical devices has revealed the shortcomings of conventional manufacturing methods in delivering products with high quality and consistency in an efficient manner (Kang and Fang, 2018). Despite new fabrication technologies being adapted to biomaterial research at an accelerating pace; few have become generally applied in industrial production. Hence, production of composite implants with continuous fibres and thermosetting matrix is still heavily centred on hand lay-up fabrication method where manual labour is in key position (Migliaresi, 2013).

In this study, the isoelastic properties compatible with those of cortical bone were aimed to achieve using spatially optimized TFP patterns with the aid of a FE-based approach. FE analysis is commonly used in biomechanical applications for analysing and optimizing stress-strain relations of complex geometries (Huiskes et al., 1992; Zhao et al., 2009; Kharazi et al., 2010). TFP is an additive manufacturing modality enabling fabrication of physical structures determined by FE or other CAD methods (Mattheij et al., 1998, Spickenheuer et al., 2008; Breier, 2015).

As anticipated, in mechanical four-point bending tests, the miniplates with unidirectional fibres promoted superior mechanical properties to the other miniplate designs based on TFP structures. However, in physiological conditions, strains contain both tensile and shear components. Under loads directed to the fibres in angles differing from orthogonal, performance of unidirectional miniplates highly relies on contact forces of the matrix material and the fibres. This makes them prone to delamination and development of inter fibre fissures. Indeed, in bending tests, the miniplates with unidirectional reinforcement were observed to develop a crack propagating through the miniplate before the eventual material failure. This collapse of the longitudinal curvature of the miniplate would implicate failure in a clinical context. To complement the tensile test, a torsion test was chosen as the other mechanical testing modality.

In torsion tests, the disintegration of unidirectionally reinforced miniplates into two or more individual pieces was emphasized. According to the torsion test, optimized TFP miniplate design provided statistically significantly higher ultimate torsion resistance as opposed to the unidirectional miniplate. This was observed with both studied material compositions of the optimized miniplate.

It was also expected that the spatial optimization would not improve the mechanical properties of the miniplates. However, even distribution of fibres within the structure and under the screw heads allowed for the creation of devices of uniform thickness. This indicates a significant improvement in the design of the device as a more stable and predictable fixation to the bone can be achieved. The improved torsional resistance

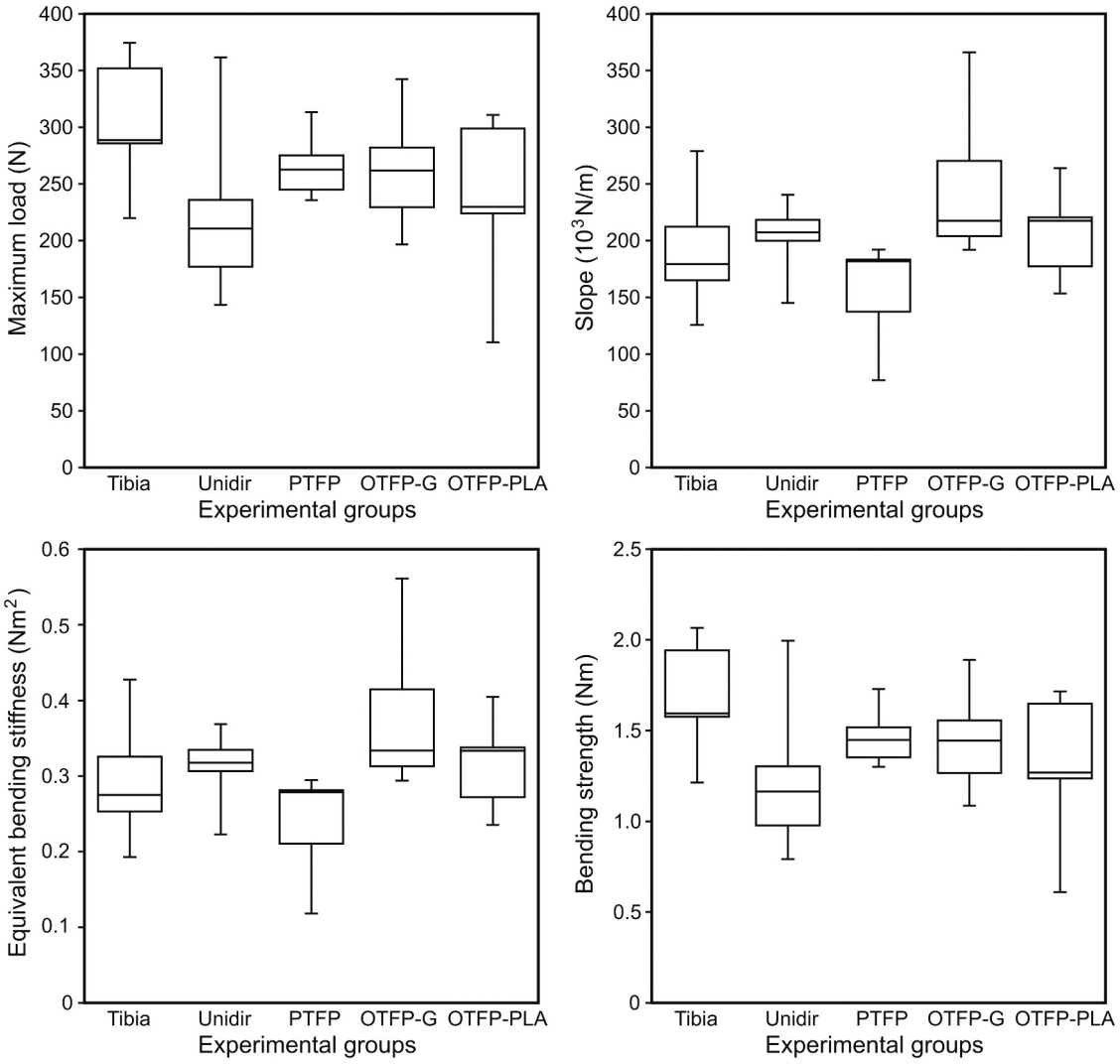

Fig. 14. Boxplots for maximum load, slope, equivalent bending stiffness, and bending strength of the constructs assessed in the four-point bending.

of the optimized TFP-based miniplate was achieved at the expense of equivalent bending stiffness and flexural strength.

Metallic fracture fixation devices have served as the golden standard for internal fracture fixation in load-bearing sites since their introduction. As their employment has several intrinsic drawbacks, novel methods for fracture treatment are sought after (Bradley et al., 1980; Tayton et al., 1982; Woo et al., 1983; Tayton and Bradley, 1983; Ali et al., 1990). As for a biomechanically ideal orthopaedic device, flexural stiffness comparable to that of cortical bone is desired along with sufficiently high flexural strength. Such device can provide the fracture site with adequate stability to promote natural ossification while minimizing adverse stress shielding effects.

The question is whether the mechanical properties of the miniplates reinforced with the TFP structures are clinically relevant? With the selected TFP-based manufacturing technique, it is impossible to base the judgment upon the properties of the material, as the material, BisGMA/TEGDMA resin matrix reinforced with continuous unidirectional *E*-glass fibres, is the same in the unidirectional and the TFP-based miniplates. Although assumptions can be made, assessment and comparison of performance should be performed at the device level. However, to our best knowledge, no standard methods seem to exist. For example, International Standard ISO 9585 is not recommended for plates with the length below 50 mm and the standard for testing small plates is still in preparation. Hence, we have to base our conclusions on circumstantial evidence obtained in mechanical tests and from the literature. The acceptable flexural strength and flexural stiffness values can be determined by comparing those of clinically applied non-metallic, polymer-based fracture fixation devices. For instance, these quantities are known to have significantly lower values in self-reinforced polylactide implants used in canine radial fracture treatment (Veiranto et al., 2002; Saikku-Bäckström et al., 2005).

In our previous study, (Liesmäki et al., 2019) a bending strength of 1006 MPa was reported for the stainless steel used in the control miniplates. On the other hand, the flexural strength of canine cortical bone was reported as 185 MPa (Acevedo et al., 2015) and 251.0 ± 49.1 MPa (Autefage et al., 2012). Bioresorbable miniplates made of poly-L/D lactide (70/30) with the flexural strength in the range of 166 to 176 MPa (Veiranto et al., 2002) were used for the fixation of distal radius fractures in toy-breed dogs (Saikku-Bäckström et al., 2005). Mechanical properties for a commercially available 6-hole plate made of commercially pure (CP grade 3) Ti intended for mandibular reconstructions were reported to be around 1000 MPa in a four-point bending (Lee et al., 2016). Consequently, materials having strength within this range of 116 to 1006 MPa could be considered as relevant for the fabrication of miniplates for the clinical applications involving load-bearing fracture fixation.

Specimens made of BisGMA/TEGDMA resin matrix reinforced with continuous unidirectional *E*-glass fibres had a flexural strength of 831

MPa while specimens made of polyether ether ketone reinforced with randomly oriented carbon fibres (CFR-PEEK) had a flexural strength of 223 MPa (Liesmäki et al., 2019). Miniplates made of these materials failed at the maximal loads of 370 N and 100 N, respectively (Liesmäki et al., 2019). It was concluded that miniplates made of both materials are adequate for clinical applications (Liesmäki et al., 2019). In this study, in line with the previous results, the maximum load for miniplates reinforced with continuous unidirectional E-glass was 373.9 N while the maximum loads in the range of 124.6–222.8 N were measured for the miniplates reinforced with the TFP structures. Consequently, one can argue that, with the same geometry, the mechanical properties of the miniplates reinforced with TFP structures should be adequate for the clinical applications involving load-bearing fracture fixation in toy-breed dogs. Importantly, unlike the miniplates reinforced with unidirectional fibres, the TFP-based miniplates did not disintegrate under loading.

Rigidity of the fracture fixation device is another important property which needs to be addressed when designing a new device. Indeed, excessive rigidity of the fracture fixation device causes unphysiological underloading, of the bone and development of plate-induced osteopenia, these conditions are acknowledged as major drawbacks of the conventional metallic fracture fixation devices (Uhthoff and Dubuc, 1971; Huiskes et al., 1992). Successful efforts made in decreasing the stress-shielding effects include applying different surgical techniques, engineering conventionally used materials into shapes with reduced structural stiffness, as well as discovering novel material choices with lower rigidity (Woo et al., 1983).

The clinical demand for fracture fixation devices with biomechanical properties comparable to those of cortical bone is emphasized in the patient groups that are especially prone to stress shielding and effects of long-term exposure to rigid plating. Such groups include individuals with pre-existing decrease in bone mineral density and impaired bone quality due to high age or underlying medical conditions, along with skeletally immature paediatric and adolescent patients (Hollevoet and Verdonk, 2003; Hollevoet et al., 2011; Kelly et al., 2013, May et al., 2013, Tinubu and Scalea, 2015). In the field of veterinary medicine, stress shielding is a notable problem among small domestic mammals (Harasen, 2003; Muir, 1997).

Evaluation of rigidity of the whole device is, however, challenging. It should be noted that modulus of elasticity is a property of a material and may not be appropriate for characterizing a device made of this material. In other words, a thinner device made of a rigid material could still be more flexible than a thicker device made of a less rigid material. Consequently, bending stiffness [Nm/deg] was widely applied to characterise and compare the rigidity of fracture fixation plates (Bradley et al., 1980; Tayton et al., 1982; Tayton and Bradley, 1983; Ali et al., 1990). Bending stiffness is determined in a four-point bending test by dividing the bending moment by the angulation of the plate during the test (Ali et al., 1990; Tayton and Bradley, 1983). In a seminal paper, Tayton and Bradley discussed the relation between the stiffness of composite plates removed from human patients and the healing of the fractures in these subjects (Tayton and Bradley, 1983). It should be noted that the plates used in that study were significantly larger than the miniplates in our study. Consequently, the set-up for the four-point bending test was different. Nevertheless, some parallels could be drawn between the two studies.

Tayton and Bradley (Tayton and Bradley, 1983) reported two types of plates made of stainless steel with the bending stiffness of 4.34 Nm/degree and 3.8 Nm/degree respectively and two types of composite plates reinforced with long carbon fibres, with the bending stiffness of 2,0 Nm/degree and 1.65 Nm/degree respectively. The geometries of the composite plates followed those of the stainless steel plates. The study also pointed out a 10% variation in the stiffness of the composite plates.

The study postulated that below the bending stiffness of 1.0 Nm/degree the plates are too flexible and there is a risk of non-union of the fracture, the minimal bending stiffness for eventless fracture healing was 1.75 Nm/degree, while the plates with the bending stiffness of 2.0 Nm/degree still produced satisfactory results (Tayton and Bradley, 1983). These findings give us reasons to believe that for composite plates, the clinically relevant bending stiffness is roughly in the range of 45–50% of the bending stiffness of the control plates made of stainless steel. While the validity of a direct comparison is questionable, it is technically possible to calculate the bending stiffness of the miniplates based on the data in this study and in our previous study (Liesmäki et al., 2019). Consequently, the bending stiffness of the miniplates in the group Unidir is 74% of that of the control miniplate made of stainless steel study (Liesmäki et al., 2019). In the group PTFP, the value is 12%, in the group OTFP-G, the value is 5% and in the group OTFP-PLA, the value is 11%. This leaves the question of rigidity of the TFP-based plates open. Apparently, further *in vitro* and *in vivo* studies are needed to clarify this issue.

Torsional strength is an important parameter for a fracture fixation device. In this respect, the approach and the respective spatial optimization of the placement of fibres performed in this study was appropriate. The study has demonstrated significant improvement in the performance of TFP-based plates over unidirectional counterparts. It is predictable that with the same amount of fibres, the reinforcement of the miniplates in torsion will compromise their performance in bending (Zhao et al., 2009; Moritz et al., 2014). Consequently, in addition to the spatial optimization performed here, a structural optimization of the TFP pattern is required. As discussed earlier, the bending stiffness of the miniplates in the group Unidir is 74% of that of the miniplates made of stainless steel. Hence, there is a margin to reduce the bending stiffness to that of 45% by placing the fibre bundles in the direction of the torsional loading.

Bending tests conducted on constructs of chicken tibiae reunited with FRC miniplates revealed no statistically significant differences. Considering the differences observed in other mechanical testing setups, this was rather unexpected. One could speculate that the lack of difference between the groups was due to the insufficient structural rigidity of the chicken bones. Indeed, as the device under development is intended for application in small mammals, especially toy-breed dogs, canine bone would have been an ideal material option for testing. However, due to the unavailability of sufficient numbers of similar bones to provide results with acceptable statistical reliability, chicken bones were selected. The chicken bones had the size and shape compatible with those of the bones of toy-breed dogs. In addition, availability of commercially available chicken drumsticks and consistent dimensions of the tibiae played the pivotal role in the selection. Another option would be to use plastic bones, but this solution would also be questionable. It should also be noted that the osteotomized bones served rather as substrates for the attachment of the miniplates than the load-bearing components of the constructs. Evidently, there are differences in the mechanical properties of mammalian and avian bones. However, there is also a significant variability in the size and morphology of canine bones (Palierne et al., 2008). It was demonstrated that the effective elastic modulus of diaphyseal cortical bone specimens was related to the breed weight and size of the animals: 13.9 GPa for the Toy Poodle to 17.2 GPa for the Doberman (Autefage et al., 2012). The average mechanical properties of canine bone specimens analysed in three-point bending were reported as 15.6 ± 2.6 GPa for effective elastic modulus, 174.3 ± 32.1 MPa for yield strength and 251.0 ± 49.1 MPa for ultimate strength (Autefage et al., 2012). How do the properties of canine cortical bone compare with those of the chicken bones? The mechanical properties of chicken tibiae were scrutinized in four-point bending tests (Regmi et al., 2017). The mean values of the elastic modulus were reported in the range of 13.15–15.41 GPa and the ultimate strength in the range of 341.73–358.12 MPa (Regmi et al., 2017). While direct comparison of the data presented in these reports is not possible, the selection of chicken bones in the context of our study was justified by the data.

5. Conclusion

The study has demonstrated the feasibility of an *in situ* contourable composite implant system applicable in load-bearing conditions, primarily intended for veterinary applications for the treatment of antebrachial fractures in toy-breed dogs. The same concept could be employed for other applications in veterinary and human patients. In addition, the study has scrutinized the application of TFP as an additive manufacturing path for the preparation of the load-bearing components of the implant system as well as applications of the TFP-based devices *per se*, as miniplates for the fixation of fractures of long bones. Biostable and bioresorbable material options were investigated. The study has demonstrated that TFP has a potential for the manufacturing of the fracture fixation devices, however, structural optimization of the patterns is required. A completely bioresorbable *in situ* contourable composite implant system and miniplates manufactured using a combination of a light-curable resin matrix (Plyusnin et al., 2021) and bioactive glass fibres (Eichhorn et al., 2021) have numerous potential applications in veterinary and human patients. Fixation of maxillofacial fractures would be of primary interest.

Acknowledgements

Dr. Cindy Elschner, Dr. Axel Spickenheuer and Dr. Lars Bittrich, Complex Structural Parts Workgroup, Department of Composite Materials, Leibniz-Institut für Polymerforschung Dresden e. V. (IPF Dresden), Dresden, Germany, are for the active role in this research work. Medical Advanced Manufacturing Research Centre (AMRC), the University of Sheffield, UK is acknowledged for the active role in this research work.

References

Acevedo, C., Bale, H., Gludovatz, B., Wat, A., Tang, S.Y., Wang, M., Busse, B., Zimmermann, E.A., Schaible, E., Allen, M.R., Burr, D.B., Ritchie, R.O., 2015. Alendronate treatment alters bone tissues at multiple structural levels in healthy canine cortical bone. Bone. 81, 352–363.

Aitasalo, K.M., Piitulainen, J.M., Rekola, J., Vallittu, P.K., 2014. Craniofacial bone reconstruction with bioactive fiber-reinforced composite implant. Head Neck 36, 722–728.

Ali, M., French, T., Hastings, G., Rae, T., Rushton, N., Ross, E., Wynn-Jones, C., 1990. Carbon fibre composite bone plates. Development, evaluation and early clinical experience. J. Bone Joint Surg. (Br.) 72-B, 586–591.

Autefage, A., Palierne, S., Charron, C., Swider, P., 2012. Effective mechanical properties of diaphyseal cortical bone in the canine femur. Vet. J. 194, 202–209.

Bradley, J.S., Hastings, G.W., Johnson-Nurse, C., 1980. Carbon fibre reinforced epoxy as a high strength, low modulus material for internal fixation plates. Biomaterials. 1, 38–40.

Breier, A.C., 2015. Embroidery technology for hard-tissue scaffolds. In: Blair, T. (Ed.), Biomedical Textiles for Orthopaedic and Surgical Applications: Fundamentals, Applications and Tissue Engineering. Elsevier, United Kingdom, pp. 23–43.

Eichhorn, J., Elschner, C., Groß, M., Reichenbächer, R., Martín, A.X.H., Soares, A.P., Fischer, H., Kulkova, J., Moritz, N., Hupa, L., Stommel, M., 2021. Spinning of endless bioactive silicate glass fibres for fibre reinforcement applications. Appl. Sci. 11, 7927.

Evans, S.L., Gregson, P.J., 1998. Composite technology in load-bearing orthopaedic implants. Biomaterials. 19, 1329–1342.

Gliesche, K., Hübner, T., Orawetz, H., 2003. Application of the tailored fibre placement (TFP) process for a local reinforcement on an "open-hole" tension plate from carbon/epoxy laminates. Compos. Sci. Technol. 63, 81–88.

Hahner, J., Hinüber, C., Breier, A., Siebert, T., Brünig, H., Heinrich, G., 2015a. Adjusting the mechanical behavior of embroidered scaffolds to lapin anterior cruciate ligaments by varying the thread materials. Text. Res. J. 85, 1431–1444.

Hahner, J., Hoyer, M., Hillig, S., Schulze-Tanzil, G., Meyer, M., Schröpfer, M., Lohan, A., Garbe, L.-A., Heinrich, G., Breier, A., 2015b. Diffusion chamber system for testing of collagen-based cell migration barriers for separation of ligament enthesis zones in tissue-engineered ACL constructs. J. Biomater. Sci. Polym. Ed. 26, 1085–1099.

Harasen, G., 2003. Common long bone fracture in small animal practice - part 2. Can. Vet. J. 44, 503–504.

Hollevoet, N., Verdonk, R., 2003. Outcome of distal radius fractures in relation to bone mineral density. Acta Orthop. Belg. 69, 510–514.

Hollevoet, N., Verdonk, R., Kaufman, J.M., Goemaere, S., 2011. Osteoporotic fracture treatment. Acta Orthop. Belg. 7, 441–447.

Hoppe, A., Güldal, N.S., Boccaccini, A.R., 2011. A review of the biological response to ionic dissolution products from bioactive glasses and glass-ceramics. Biomaterials. 32, 2757–2774.

Hoyer, M., Drechsel, N., Meyer, M., Meier, C., Hinüber, C., Breier, A., Hahner, J., Heinrich, G., Rentsch, C., Garbe, L.A., Ertel, W., 2014. Embroidered polymer–collagen hybrid scaffold variants for ligament tissue engineering. Mater. Sci. Eng. C Mater. Biol. Appl. 43, 290–299.

Huiskes, R., Weinans, H., Van Rietbergen, B., 1992. The relationship between stress shielding and bone resorption around total hip stems and the effects of flexible materials. Clin. Orthop. Relat. Res. 274, 124–134.

Kang, C.W., Fang, F.Z., 2018. State of the art of bioimplants manufacturing: part I. Adv. Manuf. 6, 20–40.

Karmaker, A.C., DiBenedetto, A.T., Goldberg, A.J., 1997. Continuous fiber reinforced composite materials as alternatives for metal alloys used for dental appliances. J. Biomater. Appl. 11, 318–328.

Kelly, B., Heyworth, B., Yen, Y.M., Hedequist, D., 2013. Adverse sequelae due to plate retention following submuscular plating for pediatric femur fractures. J. Orthop. Trauma 27, 726–729.

Kharazi, A.Z., Fathi, M.H., Bahmany, F., 2010. Design of a textile composite bone plate using 3D-finite element method. Mater. Des. 31, 1468–1474.

Kulkova Y., 2017. Bone implant. WO2017077196A1, EU patent.

Lee, J.-H., Kwon, J.-S., Moon, S.-K., Uhm, S.-H., Choi, B.-H., Joo, U.-H., Kim, K.-M., Kim, K.-N., 2016. Titanium-silver alloy miniplates for mandibular fixation: in vitro and in vivo study. J. Oral Maxillofac. Surg. 74, 1622.e1–1622.e12.

Liesmäki, O., Plyusnin, A., Kulkova, J., Lassila, L.V., Vallittu, P.K., Moritz, N., 2019. Biostable glass fibre-reinforced dimethacrylate-based composites as potential candidates for fracture fixation plates in toy-breed dogs: mechanical testing and finite element analysis. J. Mech. Behav. Biomed. Mater. 96, 172–185.

Lindfors, N.C., Koski, I., Heikkilä, J.T., Mattila, K., Aho, A.J., 2010a. A prospective randomized 14-year follow-up study of bioactive glass and autogenous bone as bone graft substitutes in benign bone tumors. J Biomed Mater Res B Appl Biomater 94, 157–164.

Lindfors, N.C., Hyvönen, P., Nyyssönen, M., Kirjavainen, M., Kankare, J., Gullichsen, E., Salo, J., 2010b. Bioactive glass S53P4 as bone graft substitute in treatment of osteomyelitis. Bone. 47, 212–218.

Mattheij, P., Gliesche, K., Feltin, D., 1998. Tailored fiber placement - mechanical properties and applications. J. Reinf. Plast. Compos. 17, 774–786.

May, C., Yen, Y.M., Nasreddine, A.Y., Hedequist, D., Hresko, M.T., Heyworth, B.E., 2013. Complications of plate fixation of femoral shaft fractures in children and adolescents. J. Child. Orthop. 7, 235–243.

Migliaresi, C., 2013. Composites. In: Ratner, B.D., Hoffman, A.S., Schoen, F.J., Lemons, J. E. (Eds.), Biomaterials Science: An Introduction to Materials in Medicine. Elsevier, Canada, pp. 223–241.

Moritz, N., Strandberg, N., Zhao, D.S., Mattila, R., Paracchini, L., Vallittu, P.K., Aro, H.T., 2014. Mechanical properties and in vivo performance of load-bearing fiber-reinforced composite intramedullary nails with improved torsional strength. J. Mech. Behav. Biomed. Mater. 40, 127–139.

Moritz, N., Mattila, R., Vallittu, P.K., 2016. Biomechanical evaluation of the load-bearing fiber-reinforced composite plates intended for the treatment of long bone fractures. In: Advances in Functional Materials; Aug 8–11; Jeju, South Korea.

Muir, P., 1997. Distal antebrachial fractures in toy breeds of dogs. Vet. Surg. 26, 254–255.

Munukka, E., Leppäranta, O., Korkeamäki, M., Vaahtio, M., Peltola, T., Zhang, D., Hupa, L., Ylänen, H., Salonen, J.I., Viljanen, M.K., Eerola, E., 2008. Bactericidal effects of bioactive glasses on clinically important aerobic bacteria. J. Mater. Sci. Mater. Med. 19, 27–32.

Muroi, N., Shimada, M., Murakami, S., Akagi, H., Kanno, N., Suzuki, S., Harada, Y., Orima, H., Hara, Y., 2021. A retrospective study of postoperative development of implant-induced osteoporosis in radial-ulnar fractures in toy breed dogs treated with plate fixation. Vet. Comp. Orthop. Traumatol. 34, 375–385.

NEWBONE, 2010. Internal Deliverable Report of WP6 D6.3 in the Framework of NEWBONE: Development of Load-Bearing Fibre Reinforced Composite Based Non-metallic Biomimetic Bone Implant. EU-funded project, Grant agreement ID: 26279, FP6-NMP Programme. https://cordis.europa.eu/project/id/26279.

Palierne, S., Mathon, D., Asimus, E., Concordet, D., Meynaud-Collard, P., Autefage, A., 2008. Segmentation of the canine population in different femoral morphological groups. Res. Vet. Sci. 85, 407–417.

Piitulainen, J.M., Posti, J.P., Aitasalo, K.M., Vuorinen, V., Vallittu, P.K., Serlo, W., 2015. Paediatric cranial defect reconstruction using bioactive fibre-reinforced composite implant: early outcomes. Acta Neurochir. 157, 681–687.

Plyusnin, A., He, J., Elschner, C., Nakamura, M., Kulkova, J., Spickenheuer, A., Scheffler, C., Lassila, L.V.J., Moritz, N., 2021. A polymer for application as a matrix phase in a concept of in situ curable bioresorbable bioactive load-bearing continuous fiber reinforced composite fracture fixation plates. Molecules. 26, 1256.

Ramakrishna, S., Mayer, J., Wintermantel, E., Leong, K.W., 2001. Biomedical applications of polymer-composite materials: a review. Compos. Sci. Technol. 61, 1189–1224.

Regmi, P., Nelson, N., Haut, R.C., Orth, M.W., Karcher, D.M., 2017. Influence of age and housing systems on properties of tibia and humerus of Lohmann white hens: bone properties of laying hens in commercial housing systems. Poult. Sci. 96, 3755–3762.

Rentsch, C., Rentsch, B., Breier, A., Spekl, K., Jung, R., Manthey, S., Scharnweber, D., Zwipp, H., Biewener, A., 2010. Long-bone critical-size defects treated with tissue-engineered polycaprolactone-co-lactide scaffolds: a pilot study on rats. J. Biomed. Mater. Res. A 95, 964–972.

Rentsch, C., Schneiders, W., Hess, R., Rentsch, B., Bernhardt, R., Spekl, K., Schneider, K., Scharnweber, D., Biewener, A., Rammelt, S., 2014. Healing properties of surface-coated polycaprolactone-co-lactide scaffolds: a pilot study in sheep. J. Biomater. Appl. 28, 654–666.

Saikku-Bäckström, A., Tulamo, R.M., Räihä, J.E., Kellomäki, M., Toivonen, T., Törmälä, P., Rokkanen, P., 2000. Intramedullary fixation of cortical bone osteotomies with absorbable self-reinforced fibrillated poly-96L/4D-lactide (SR-PLA96) rods in rabbits. Biomaterials. 22, 33–43.

Saikku-Bäckström, A., Räihä, J.E., Välimaa, T., Tulamo, R.M., 2005. Repair of radial fractures in toy breed dogs with self-reinforced biodegradable bone plates, metal screws, and light-weight external coaptation. Vet. Surg. 34, 11–17.

Sod, G.A., Hubert, J.D., Martin, G.S., Gill, M.S., 2005. An in vitro biomechanical comparison of a limited-contact dynamic compression plate fixation with a dynamic compression plate fixation of osteotomized equine third metacarpal bones. Vet. Surg. 34, 579–586.

Spickenheuer, A., Schulz, M., Gliesche, K., Heinrich, G., 2008. Using tailored fibre placement technology for stress adapted design of composite structures. Plast. Rubber Compos. 37, 227–232.

Tayton, K., Bradley, J., 1983. How stiff should semi-rigid fixation of the human tibia be? A clue to the answer. J. Bone Joint Surg. (Br.) 65-B, 312–315.

Tayton, K., Johnson-Nurse, C., McKibbin, B., Bradley, J., Hastings, G., 1982. The use of semi-rigid carbon-fibre-reinforced plastic plates for fixation of human fractures. Results of preliminary trials. J. Bone Joint Surg. (Br.) 64, 105–111.

Tinubu, J., Scalea, T.M., 2015. Management of fractures in a geriatric surgical patient. Surg. Clin. North Am. 95, 115–128.

Tuusa, S.R., Peltola, M.J., Tirri, T., Lassila, L.V.J., Vallittu, P.K., 2007. Frontal bone defect repair with experimental glass-fiber-reinforced composite with bioactive glass granule coating. J Biomed Mater Res B Appl Biomater 82, 149–155.

Tuusa, S.M.R., Peltola, M.J., Tirri, T., Puska, M.A., Röyttä, M., Aho, H., Sandholm, J., Lassila, L.V.J., Vallittu, P.K., 2008. Reconstruction of critical size calvarial bone defects in rabbits with glass–fiber-reinforced composite with bioactive glass granule coating. J Biomed Mater Res B Appl Biomater 84, 510–519.

Uhthoff, H.K., Dubuc, F.L., 1971. Bone structure changes in the dog under rigid in-ternal fixation. Clin. Orthop. Relat. Res. 81, 165–170.

Vallittu, P.K., 1999. Flexural properties of acrylic resin polymers reinforced with unidirectional and woven glass fibers. J. Prosthet. Dent. 81, 318–326.

Vallittu, P.K., 2017. Bioactive glass-containing cranial implants: an overview. J. Mater. Sci. 52, 8772–8784.

Veiranto, M., Törmälä, P., Suokas, E., 2002. In vitro mechanical and drug release properties of bioabsorbable ciprofloxacin containing and neat self-reinforced P (L/DL) LA 70/30 fixation screws. J. Mater. Sci. Mater. Med. 13, 1259–1264.

Woo, S., Lothringer, K.S., Akeson, W.H., Coutts, R.D., Woo, Y.K., Simon, B.R., Gomez, M. A., 1983. Less rigid internal fixation plates: historical perspectives and new concepts. J. Orthop. Res. 1, 431–449.

Yang, P.F., Sanno, M., Ganse, B., Koy, T., Brüggemann, G.P., Müller, L.P., Rittweger, J., 2014. Torsion and antero-posterior bending in the in vivo human tibia loading regimes during walking and running. PLoS One 9 (4), e94525.

Zhao, D.S., Moritz, N., Laurila, P., Mattila, R., Lassila, L.V.J., Strandberg, N., Mäntylä, T., Vallittu, P.K., Aro, H.T., 2009. Development of a multi-component fiber-reinforced composite implant for load-sharing conditions. Med. Eng. Phys. 31, 461–469.